

Improved simulation of phase change processes in applications where  
conduction is the dominant heat transfer mode

**B.L. Gowreesunker<sup>\*</sup>, S.A. Tassou, M. Kolokotroni**

*Howell Building, Mechanical Engineering, School of Engineering and Design, Brunel  
University, Uxbridge, Middlesex, UB8 3PH, UK*

\* Corresponding Author: Baboo.Gowreesunker@brunel.ac.uk

United Kingdom

**Abstract:**

This paper reports on the development, experimental validation and application of a semi-empirical model for the simulation of the phase change process in phase change materials (PCM). PCMs are now increasingly being used in various building materials such as plasterboard, concrete or panels to improve thermal control in buildings and accurate modelling of their behaviour is important to effectively capture the effects of storage on indoor thermal conditions. Unlike many commercial simulation packages that assume very similar melting and freezing behaviour for the PCM and no hysteresis, the methodology employed treats the melting and freezing processes separately and this allows the inclusion of the effect of hysteresis in the modelling. As demonstrated by the results in this paper, this approach provides a more accurate prediction of the temperature and heat flow in the material, which is of particular importance in providing accurate representation of indoor thermal conditions during thermal cycling. The difference in the prediction accuracy of the two methods is a function of the properties of the PCM. The smaller the hysteresis of the PCM, the lower will be the prediction error of the conventional approach, and solution time will become the determining factor in selecting the simulation approach in practical applications.

**Keywords:** Phase Change Materials (PCM), Heat source/sink, Temperature hysteresis

**Nomenclature:**

$t$	Time (s)
$\rho$	Density (kg/m <sup>3</sup> )
$H$	Enthalpy (J/kg)
$u_j$	Velocity vector
$\lambda$	Thermal conductivity (W/m K)
$T$	Temperature (K)
$x_j$	Direction vector
$\beta$	Liquid Fraction
$c_p$	Specific heat capacity (J/Kg K)
$L$	Latent heat capacity (J/kg)
$\Delta t$	Time step (s)
$h_{ref}$	Reference enthalpy (J/kg)
$f(T)$	User Defined Cumulative energy v/s Temperature relation

**Subscripts:**

$sol$	<i>Solidus</i>
$liq$	<i>Liquidus</i>
$m$	<i>Melting</i>
$f$	<i>Freezing</i>
$t$	<i>Current time</i>
$t-1$	<i>Previous time</i>
$ref$	<i>Reference values</i>

## 1.0 Introduction

Phase change materials (PCM), in the context of buildings, refer to materials with enhanced heat storage capabilities in a specific temperature range through accessing the latent capacity of the materials. Conventional building materials such as bricks and concrete provide thermal mass by sensible processes, that is, through changes in temperature. However the growing trend by architects to design aesthetically pleasing buildings, with maximum exposure to the outdoors and maximum sunlight, produces thermally less massive buildings and therefore reduces the influence of the thermal inertia of the building on indoor environment, leading to higher energy consumption.

Various studies have portrayed PCMs as a very effective way of enhancing the thermal inertia properties of lightweight building materials [1,2]. Kuznik et al. [3] showed that a 5 mm thick 60% micro-encapsulated paraffin PCM wallboard stored energy equivalent to 8 cm thick concrete. The increased interest in PCMs has led to various companies developing commercial products for new or retrofit applications. Such products include BASF Micronal<sup>(r)</sup> PCM boards, DuPont Energain<sup>(r)</sup> the EBB Clay PCM building boards, as well as a growing number of experimental prototypes [12].

While the advantages of PCMs are clear, their effectiveness is heavily dependent on the building fabric, weather conditions and their interaction with heating, ventilation and air-conditioning equipment. Numerical modelling provides a way of establishing the performance of PCMs over a wide range of conditions and operating modes. Various commercial simulation tools incorporate phase change modelling capabilities such as ESP-r [10]; TRNSYS [11]; and FLUENT, amongst others. However, these simulation tools do not provide a flexible enough way to introduce custom individual melting and freezing

processes. The validation of the heat source/sink method used in this study to overcome these limitations will be performed with FLUENT, even though it can also be applied using other commercial CFD packages, via the governing energy equation.

Computational Fluid Dynamics (CFD) simulation environments usually possess a default melting/solidification model but this does not provide the flexibility to vary the enthalpy-temperature relationships and the possibility of introducing temperature hysteresis [4]. The default enthalpy-porosity method used, developed from the Stefan Problem, does not explicitly track the solid-liquid interface, but rather, a parameter known as the liquid fraction ( $\beta$ ), which indicates the fraction of liquid in a specific cell in the modelling domain [5]. The liquid fraction allows the computation of the change in enthalpy from the energy in the material during phase change as follows [6].

$$\frac{d}{dt}\rho H = -\frac{d}{dx_j}\rho u_j c_p T + \frac{d}{dx_j}\left[\lambda \frac{dT}{dx_j}\right] + S_E \quad \text{Eq. (1)}$$

$$\left. \begin{aligned} \beta &= 0 ; T < T_{sol} \\ \beta &= \frac{T - T_{sol}}{T_{liq} - T_{sol}} ; T_{sol} < T < T_{liq} \\ \beta &= 1 ; T > T_{liq} \end{aligned} \right\} \quad \text{Eqs. (2)}$$

Where;

$$H = h_{ref} + \int_{T_{ref}}^T c_p dT + \beta L \quad \text{Eq. (3)}$$

The solver constantly iterates between Eq. (1) and (3) to determine the temperature of each cell. In conduction dominant materials where advective movements within the liquid phase are negligible, Eq. (1) can be simplified to:

$$\frac{d}{dt} \rho H = \frac{d}{dx_j} \left[ \lambda \frac{dT}{dx_j} \right] + S_E \quad (4)$$

The limitations of the default enthalpy-porosity model presented above are that the calculation of the liquid fraction is done via the lever rule [6] (that is, the enthalpy/temperature relationships are assumed linear), and that the solver assumes that the melting and solidification enthalpy-temperature relationships are similar. Previous observations show that these are not always the case, and can result in discrepancies between experimental and numerical results [4, 7, 9].

This paper presents an approach by which the process of melting and solidification are treated separately by using specific enthalpy-temperature relationships of melting and solidification within the CFD model. This provides a better representation of the processes involved and more accurate simulation results. This method is inspired by similar works performed on evaporation/condensation [8]. The concept relies on the addition of a heat source term  $S_E$  in equation (4) to mimic the melting and solidification process. The works in ref. [8] focus on a single phase change temperature, incorporating source terms in the energy and momentum equations to simulate phase change in pure water. This study, on the other hand, focuses on phase change temperature ranges (mushy regions) and only influences the energy equation.

Contrary to the methods in commercial software, such as FLUENT which uses the enthalpy-porosity method, the method proposed here calculates the energy stored/released directly from the temperature in the form of a user defined function (UDF). The liquid fraction is calculated as an extra parameter, also from a UDF, but is not used in the simulation process.

This eliminates the dependency of the enthalpy function to obey the lever rule and provides a more flexible approach.

This method may be considered as an extrapolation of the enthalpy-porosity method, even though it uses a heat source/sink as opposed to the explicit enthalpy-temperature relation. The reason is that the quantification of the heat source/sink is dependent on the energy or enthalpy change during the phase change process. This, therefore, is a semi-empirical method requiring the experimental enthalpy-temperature relation to be determined through thermal techniques such as Differential Scanning Calorimetry (DSC) [4] or the T-history method [13].

The approach presented in this study is valid for materials where advective movements inside the PCM are negligible and the dominant heat transfer mode is conduction. This is the case for PCMs impregnated in matrices such as plasterboard or tiles. In applications where large quantities of PCM are used, for example PCM in large tank for thermal storage applications, movement of the liquid phase will introduce heat transfer by convection. In these cases, the source term in Eq. 1 must be modified to accommodate for the appropriate convection effects.

## 2.0 Description of the model

A crucial aspect of the model is to differentiate between melting and freezing, so that the solver uses the appropriate heat source function. Melting is an endothermic process, i.e. absorbing heat as the temperature of the material increases, and freezing is an exothermic process, releasing heat as the temperature decreases. As a result, melting will be mimicked through a heat sink, while freezing as a heat source, with the corresponding change in temperature, incorporated in the source term  $S_E$  in Eq. (4).

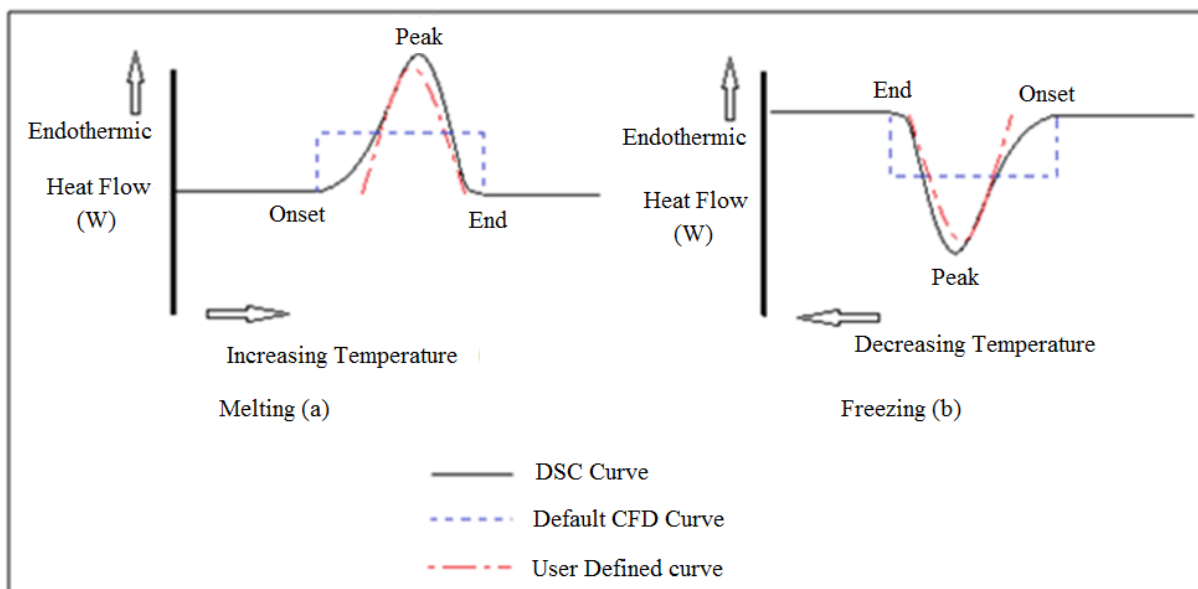


Fig. 1 - Differences between the step function used in commercial software to describe melting and freezing, actual data from DSC results, and data produced by the modelling approach proposed in this paper.

It can be seen from Fig. 1 that the default CFD curve is a step function, approximating the DSC curve. The default CFD curve aims at equalising the area between the onset and the end points, and is not an accurate representation of the actual DSC curve. On the other hand, the UDF ( $S_E$ ) is a more flexible, accurate representation of the DSC curve. By

appropriately adjusting the regression coefficient of the UDF polynomial curve, an exact representation of the DSC can be obtained, depending on the material properties.

For melting, the simulation cell temperature at the previous time-step should be lower than at the 'actual' time-step, and vice-versa for freezing. This concept is therefore used to provide the solver with the required information to determine whether the material in a specific cell is melting or freezing, and consequently follow the appropriate enthalpy-temperature curve. Additionally, the function of the liquid fraction can be defined based on the curvature of the integral of the UDF DSC curve, and the onset and end temperatures of the phase change.

For completeness, it is not sufficient to define the heat source term ( $S_E$ ) only inside the phase change temperature range; it should also be defined for all the conditions in Table 1.

(Note that  $T_{sol} < T_{liq}$ )

Heat sink conditions for Melting ( $T_{t-1} < T_t$ )	
$(T_t \leq T_{liq,m}) \& (T_{t-1} \geq T_{sol,m})$	$S_{E,m} = -\frac{\rho}{\Delta t} \int_{T_{t-1}}^{T_t} f(T)_m dT$ - Eq.(5)
$(T_t > T_{liq,m}) \& (T_{t-1} < T_{sol,m})$	$S_{E,m} = -\frac{\rho}{\Delta t} L$ - Eq.(6)
$(T_{sol,m} \leq T_t \leq T_{liq,m}) \& (T_{t-1} < T_{sol,m})$	$S_{E,m} = -\frac{\rho}{\Delta t} \int_{T_{sol}}^{T_t} f(T)_m dT$ - Eq.(7)
$(T_t > T_{liq,m}) \& (T_{sol,m} \leq T_{t-1} \leq T_{liq,m})$	$S_{E,m} = -\frac{\rho}{\Delta t} \int_{T_{t-1}}^{T_{liq}} f(T)_m dT$ - Eq.(8)
Heat source conditions for Freezing ( $T_{t-1} > T_t$ )	
$(T_t \geq T_{sol,f}) \& (T_{t-1} \leq T_{liq,f})$	$S_{E,f} = \frac{\rho}{\Delta t} \int_{T_{t-1}}^{T_t} f(T)_f dT$ - Eq.(9)
$(T_t < T_{sol,f}) \& (T_{t-1} > T_{liq,f})$	$S_{E,f} = \frac{\rho}{\Delta t} L$ - Eq.(10)
$(T_{sol,f} \leq T_t \leq T_{liq,f}) \& (T_{t-1} > T_{liq,f})$	$S_{E,f} = \frac{\rho}{\Delta t} \int_{T_{liq}}^{T_t} f(T)_f dT$ - Eq.(11)
$(T_t < T_{sol,f}) \& (T_{sol,f} \leq T_{t-1} \leq T_{liq,f})$	$S_{E,f} = \frac{\rho}{\Delta t} \int_{T_{t-1}}^{T_{sol}} f(T)_f dT$ - Eq.(12)
Liquid Fraction ( $\beta$ )Conditions	
Melting & Freezing: ( $T_{sol} \leq T_t \leq T_{liq}$ )	

Table 1- Conditions required to fully defining the heat source/sink User Defined Source term.  $f(T)_m$  and  $f(T)_f$  are the equations of the cumulative energy (J/kg) against temperature relationships from the UDF DSC curve in Fig. 1, from the onset of melting and freezing, respectively.

### 3.0 Experimental Setup

The experimental setup consisted of macro-encapsulating the PCM material in a 100mm × 70 mm × 80mm aluminium box as shown in Fig. 2. The box consisted of approximately 0.5 kg of the composite PCM. The material investigated is a composite of low density polyethylene and organic PCM, with phase change behaviour as shown in Fig. 4. The experiment was conducted in an environmental chamber, with 4 T-type thermocouples (located as shown in

Fig. 2) and a PICO data logger, calibrated for the temperature range encountered in the experiment.

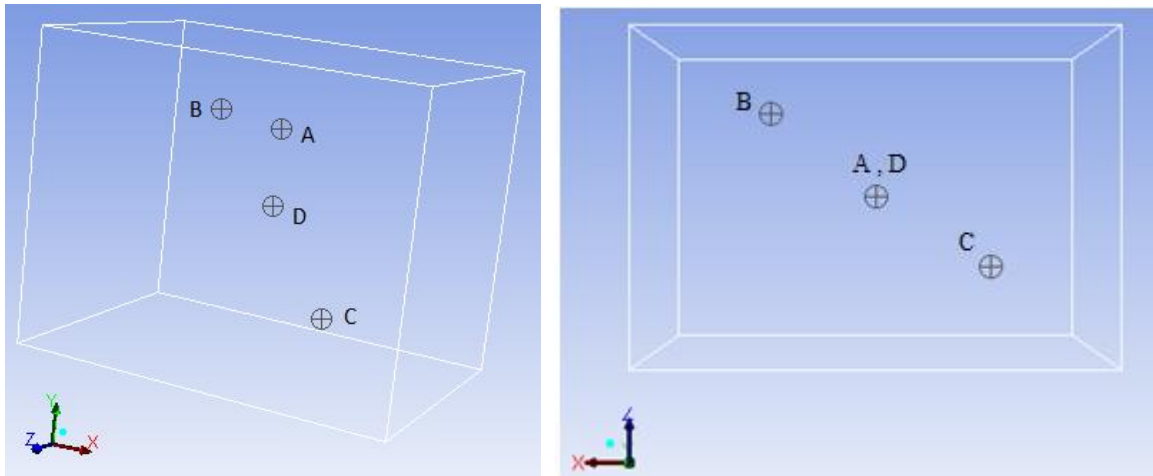


Fig. 2 - Box with thermocouple locations

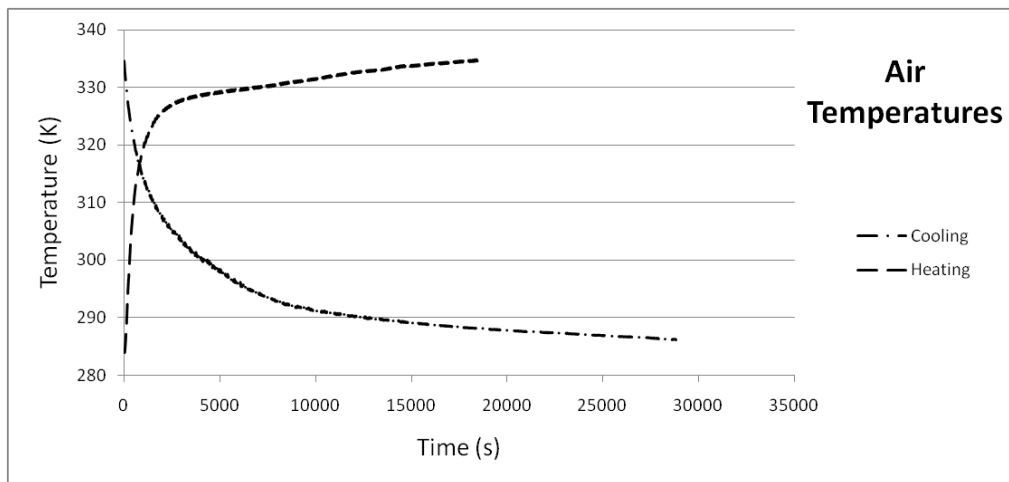


Fig. 3 - Experimental Air Temperature variations

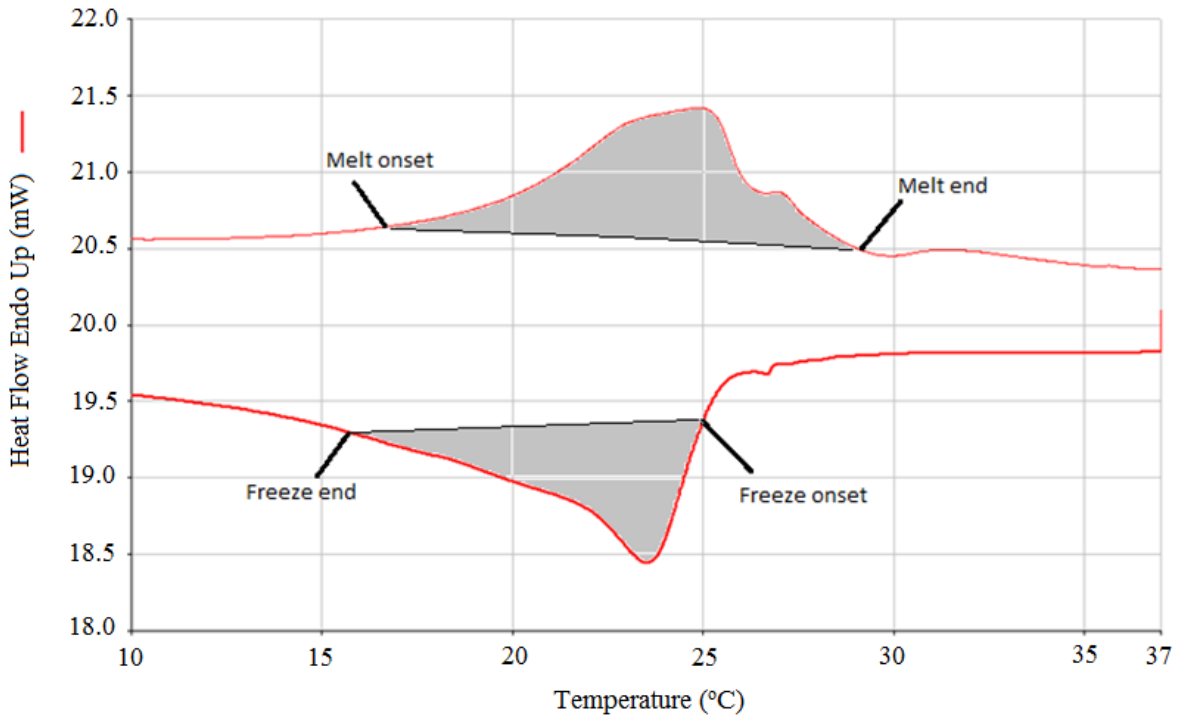


Fig. 4 - DSC result of PCM composite

The shaded areas underneath the DSC curves represent the latent heat energy during phase change used in this study. Note that freezing is slightly underestimated in order to portray the effect of inaccurately choosing the phase change parameters (onset and end temperatures and latent heat capacity). More details are given in section 4.0.

The air temperature of the chamber was varied from below the solidus temperature and above the liquidus temperature as shown in Fig. 3, and the temperature at different points in the composite was recorded at intervals of 5 s.

#### 4.0 Model inputs

The physical and thermal properties of the composite PCM material shown in Table 2 were obtained from the manufacturer.

Density	840 kg/m <sup>3</sup>
Specific heat capacity	2400 J/kgK
Thermal conductivity	0.3 W/mK

Table 2 - Manufacturer's PCM properties

Following the DSC curves in Fig. 4, the cumulative energy for the PCM composite for melting and freezing are shown in Fig. 5. It is important to note that DSC provides the heat flow (mW) at each temperature for a specific sample mass, and that these values have to be properly converted to energy (J/kg) in order to be compatible in this method.

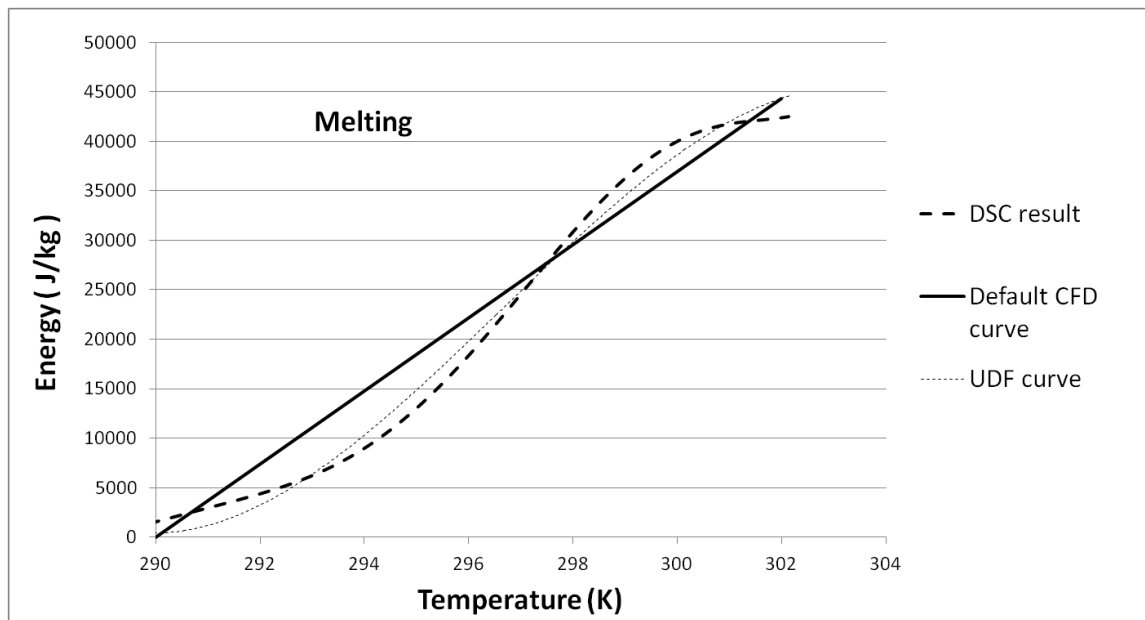


Fig. 5(a) - Experimental, UDF & Default CFD cumulative energy-temperature curves for the melting process

The cumulative energy curve shown in Fig. 5(a) (equivalent to the enthalpy/energy-temperature relation) provides the basis for the melting process. The onset of melting is taken to be 290 K (16.85 °C) and the end temperature 302 K (28.85 °C), with a latent heat capacity of 44360 J/kg, based on the original DSC curves in Fig 4. The equation (J/kg) of the UDF curve is given by:

$$f(T)_m = -38.24 T^3 + 34027.22 T^2 - 10088202.17 T + 996484631.17 \quad (R^2 = 0.992) \quad - \text{Eq. (13)}$$

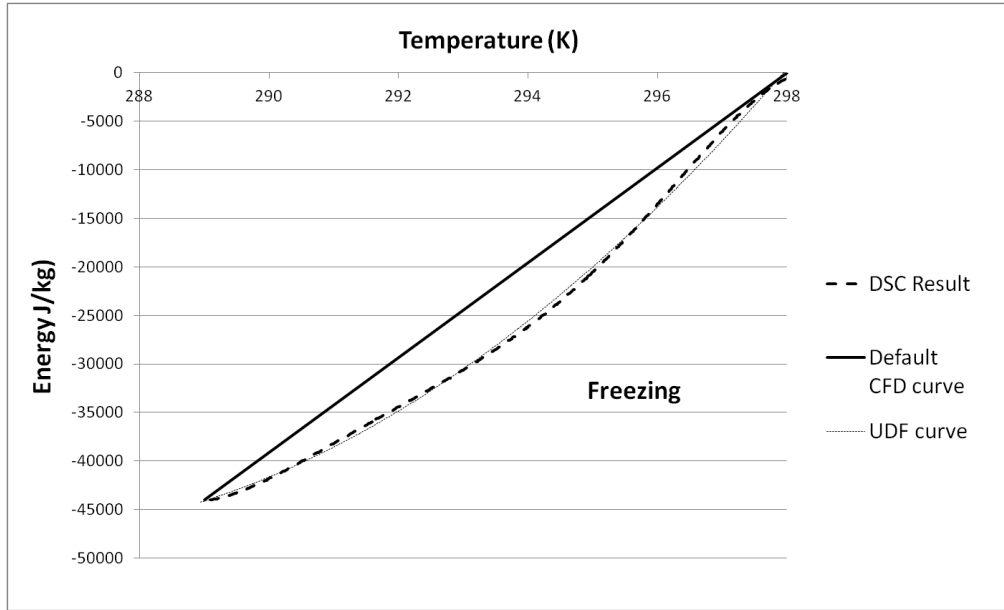


Fig. 5 (b) - Experimental, UDF & Default CFD cumulative energy-temperature curves for freezing process

Similarly, the onset of freezing is taken to be 298.15 K (25.00 °C) and the end temperature at 289 K (15.85 °C), producing an average hysteresis of  $\approx 2$  K, based on the energy curves. The latent heat capacity for freezing is 44117 J/kg. The equation of the UDF curve (J/kg) was determined to be:

$$-f(T)_f = -0.10 T^3 + 394.48 T^2 - 201586.68 T + 27601496.40 \quad (R^2 = 0.997) \quad - \text{Eq. (14)}$$

The liquid fraction equations for melting and freezing respectively are:

$$\beta_m = -0.001 T^3 + 0.767 T^2 - 227.412 T + 22463.113 \quad - \text{Eq. (15)}$$

$$\beta_f = 0.007 T^2 - 3.769 T + 537.874 \quad - \text{Eq. (16)}$$

## 5.0 Validation & Discussion

Validation of the model was done in two parts; melting and freezing. This is to provide greater flexibility in the simulations, as well as to ease the investigation of the model in regards to melting and freezing separately. The modelling results are obtained with a mesh-

converged model of 12,320 hexahedral elements, a converged time-step of 10s and all simulations iteratively converged. The validation results are shown for a single point, in the material domain, although the same trends and explanations apply to all other points.

### 5.1 Melting Process

For melting, the PCM box is initialised at 8°C and the air temperature gradually increases with the same trend as in the experiment. A convective heat transfer coefficient of 5 W/m<sup>2</sup>K between the box and the surrounding air is used for validation. The temperatures at the four locations were monitored. The validation results for location A are shown in Fig. 6.

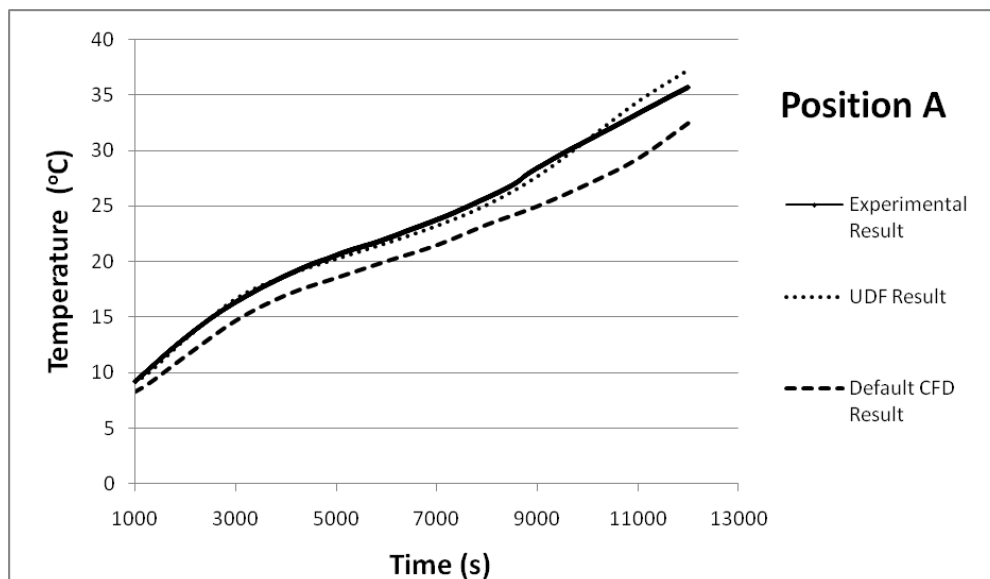


Fig. 6 - Experimental, UDF model and Default CFD model temperatures of point A during the melting process

The results in Fig. 6 show the differences in using the different models in relation to the experiment. The UDF model predicts the temperature trend at both points more accurately than the default FLUENT model. From the energy-temperature curve in Fig. 5(a), the UDF model produces a gradual energy change, as opposed to the default model where the energy change is constant. Furthermore, the onset and the end temperatures of melting on both models are accurate, confirming the reliability in the approximation of the DSC energy

curve. The difference towards the end of the simulation time (> 9000s) can be attributed to an increase in specific heat capacity as the material changes from solid to liquid phase. This change in  $c_p$  was not incorporated in the models.

The default FLUENT model predicts lower temperatures for both locations during melting. Close attention to the models' results in Fig. 6 shows that if the initial temperature trends during melting are flawed, then the error is carried into the simulation affecting results at later times, providing incorrect system thermal dynamics.

For ease of comparison, the Root Mean Square (RMS) errors relative to the experimental data were calculated for each location. For the case of melting, the UDF model produced an error of 1.3%, while the Default CFD model produced a much higher error of 12.3%, and therefore confirming the prediction accuracy of the UDF model.

## 5.2 Freezing Process

For freezing, the PCM box is initialised at 59°C and the air temperature gradually decreases with the same trend as in the experiment. A convective heat transfer coefficient of 8 W/m<sup>2</sup>K between the box and the surrounding air, and a specific heat capacity of 2550 J/kgK are used for validation. The validation results for locations C are shown in Fig. 7.

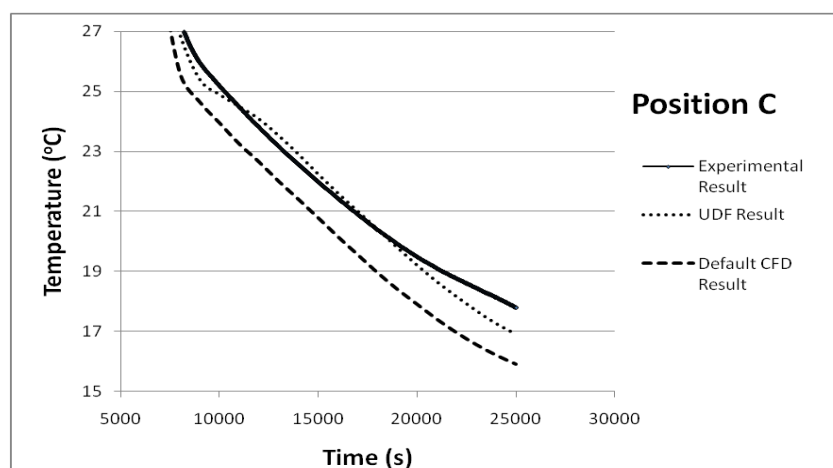


Fig. 7 - Experimental, UDF and Default CFD models' temperatures of point C during the freezing process

The results from Fig. 7 show that the experimental approximation of the energy-temperature curve in Fig. 5 (b) is not accurate enough to exactly predict the freezing temperature trends in the composite. This is due to the fact that a slightly inaccurate freezing onset temperature and energy-temperature curve were deliberately chosen from the DSC data (Fig. 4). Therefore, the discrepancy at the initial stages of freezing in the UDF model in Fig. 7, is due to a sharper gradient in the UDF energy-temperature curve, relative to the DSC results, at the onset of freezing (298 K) in Fig. 5(b). The temperature trend in Fig. 7 of the UDF model is however a good representation of the UDF energy-temperature curve input.

Conversely, the default CFD model predicts a temperature trend with an average error of approximately 2°C over the freezing range. Thus, even with a relatively inaccurate selection of the UDF enthalpy-temperature relationship, the UDF model provides a more accurate prediction than the default model. In this case, the RMS error for the UDF model is 0.5%, while the default model produces a much higher error of 6.3%, over the phase change range.

The main observation from sections 5.1 and 5.2 is that the errors with the UDF model are lower than the default CFD model for both the melting and freezing cases.

### *5.3 Validation Contour plots of UDF model for Melting and Freezing*

Figs. 8 and 9 show the contour plots of the PCM composite during the melting and freezing processes using the UDF model. Melting completes after 12000s while freezing is a much

slower process (due to slower reduction in the surrounding experimental air temperature), and completes in more than 20000s. The phase change effects start at the corners and edges due to higher heat transfer rates and progresses towards the bulk of the composite. The contour results, depicted in Figs. 8 and 9 for both the temperatures and the liquid fraction for melting and freezing, respectively, are in accordance with the user defined functions. Figs. 8 and 9 show five plane sections of the entire 3-D PCM model simulated, and confirm the validity of the UDF model in regards to visualisation of heat transfer. In this case where the advective movements are neglected, the liquid fraction does not affect the momentum of the liquid phase of the PCM. It is simply aids visualisation of the mushy parts.

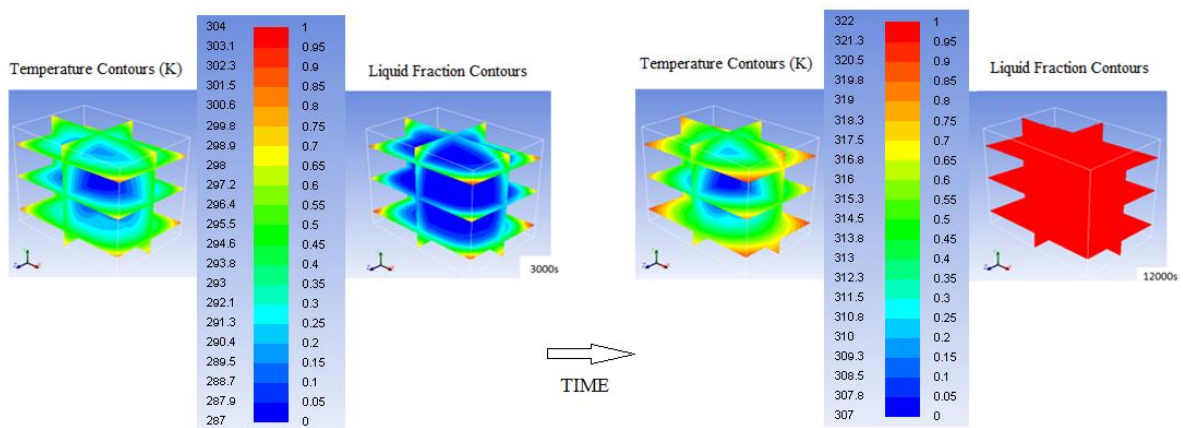


Fig. 8 - Temperature and Liquid Fraction contours during the melting process

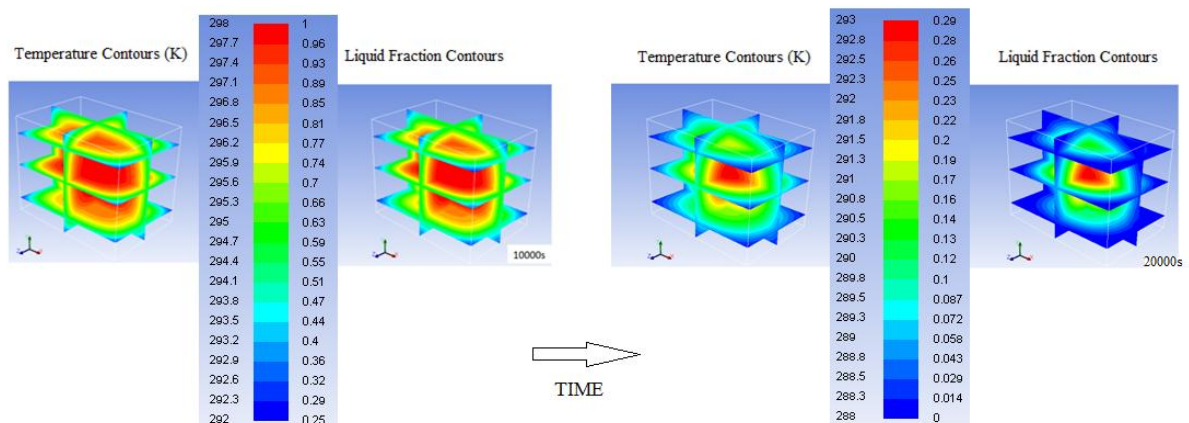


Fig. 9 - Temperature and Liquid Fraction contours during the freezing process

## 6.0 Application of heat source/sink model

PCMs are a growing technology used in buildings to provide passive thermal control of the indoor environment, by introducing additional thermal inertia in the internal space to lower the air temperature swing, and maintain thermal comfort. Commercial products include BASF Micronal<sup>(r)</sup> PCM boards, DuPont Energain<sup>(r)</sup> and the EBB Clay PCM building boards. To test the performance of such systems, numerical simulations are often employed, but as shown in Figs. 6 and 7, using the default enthalpy-porosity models of phase change often leads to errors in the dynamic temperature predictions. The following sub-sections will portray the use of the heat source/sink model, in comparison to the default CFD model for an average lightweight external wall.

The wall consists of 19mm render, 200mm concrete and 13mm plaster, and according to CIBSE [14], has a decrement factor of 0.42 and decrement delay of 6.5 hrs. To this wall, a 20mm solid PCM layer was applied on the internal side, and the thermal response of the wall examined with both the heat source/sink model and the default enthalpy-porosity model. The walls were investigated in FLUENT by applying a sinusoidal air temperature excitation: varying from peak temperatures of 273.15K and 318.15K, over a period of 24 hours, with heat transfer coefficient of 7.7 W/m<sup>2</sup>K on the internal surface [14], and the external surfaces maintained as adiabatic, as shown in Fig. 10.

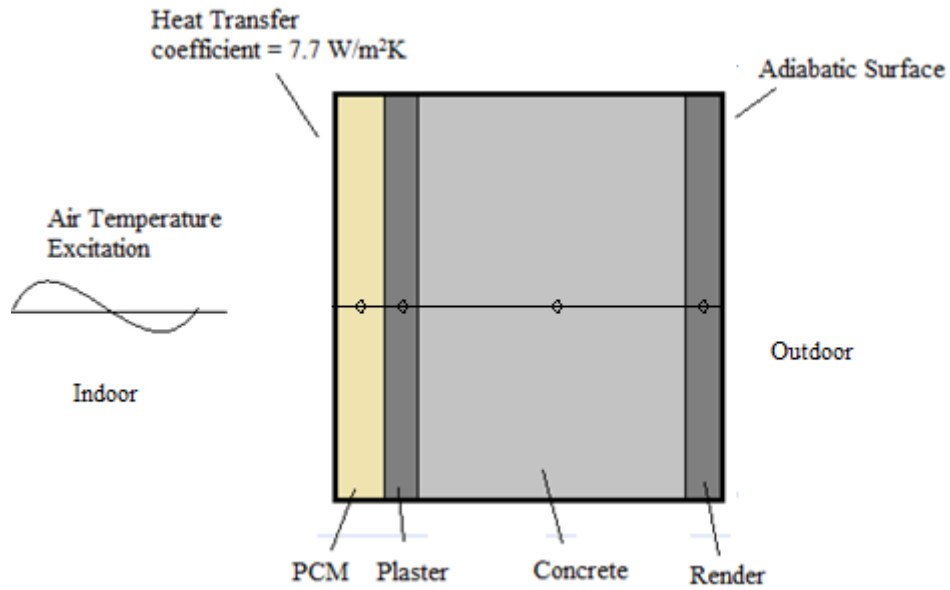


Fig. 10 – Simulation Wall Description

The PCM used for the validation of the heat source/sink model (Fig. 4) is used for this non-linear energy-temperature relationship investigation. The PCM thermal properties can be obtained from Figs. 4 and 5, and Table 2. Because of the inability to specify separate melting and freezing temperatures and enthalpies in the default model, the solidus temperature was taken to be 289.5 K, the liquidus temperature as 300.1 K and the latent heat capacity as 44240 J/kg, calculated as the average values for both melting and freezing.

Fig. 11 shows the temperature variation with time at the midpoints of each wall layer, predicted by the default method in the CFD software and from the User Defined Model, for one air temperature cycle.

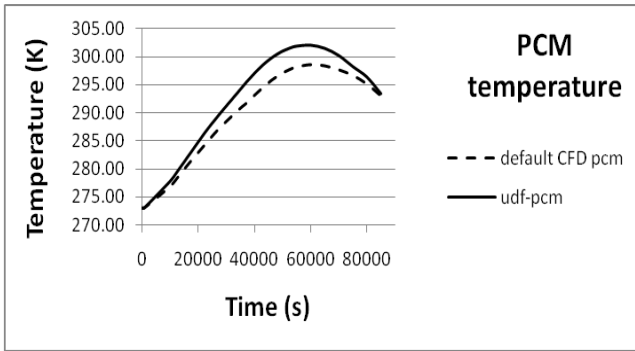


Fig. 11(a) – PCM temperature development

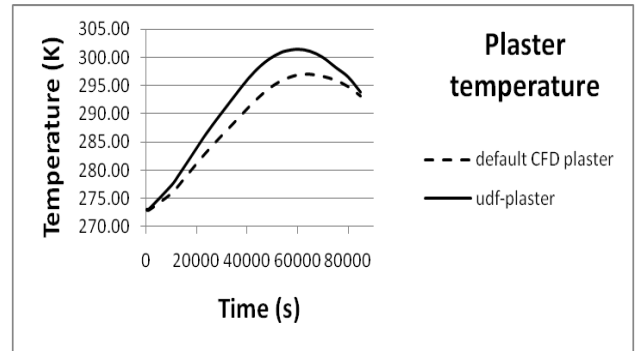


Fig. 11(b) – Plaster temperature development

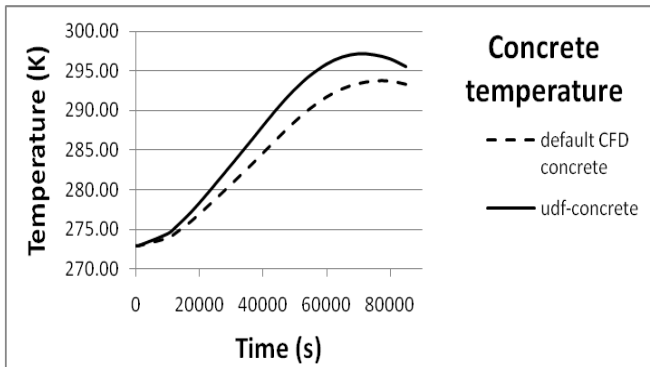


Fig. 11(c) – Concrete temperature development

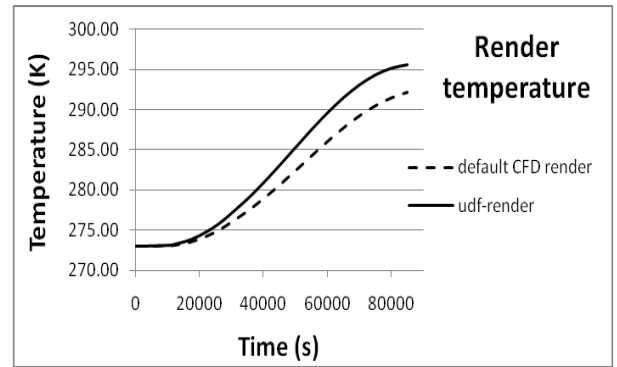


Fig. 11(d) – Render temperature development

Fig. 11 – Simulated temperature trends at midpoints of simulation wall for validation PCM

Figs. 11 (a) – (d) show that the thermal dynamics of the entire wall is affected by the choice of the phase change model. The phase change temperature trend in the PCM segment of the wall (Fig. 11a) are in accordance with the individual model (default and UDF) enthalpy-temperature curves, but the thermal dynamics of the entire wall is very different for each model, with peak temperature differences of approximately 4 – 5 K.

As the default model assumes a higher enthalpy change at the beginning of melting (Fig. 5a), the temperatures in the UDF model (Fig. 11a) are higher, due to the lower latent heat storage capacity of the PCM. Subsequently, the onset of freezing is clearly shown in Fig. 11(a) at  $t \approx 70000$ s by the change in temperature reduction rate for the UDF model, in relation to the gradual change in the default model. It is noticed that the initial temperature trends in the wall are very important in the subsequent development of temperature along

the materials. In this regard, the curvatures of the enthalpy-temperature relationships are very important, as they dictate both the initial and subsequent development of temperature in not only the PCM layer, but in the entire wall.

## **7.0 Conclusion**

The results in the paper show that the heat source/sink method developed is suitable for the prediction of phase change phenomena and offers more accurate representation of the temperature during phase change processes compared to the default enthalpy-porosity method used by many commercial software packages. The importance of energy variation with temperature during phase change and its direct effect to the solution dynamics in a wall are portrayed. Furthermore, because the individual melting and freezing effects as well as hysteresis are incorporated in the same code, this method allows accurate simulation of the PCM behaviour under cyclic conditions imposed by the variation in external ambient temperature.

As CFD simulations require detailed inputs, this semi-empirical model is also heavily dependent on the thermal properties of the PCM, especially the temperatures at the start and end of the melting and freezing processes, the energy-temperature relations as well as the specific heat-temperature relations. Variation of the thermal conductivity of the PCM with temperature may also have an influence if significant changes in its value take place during phase change. Hence, the input to the simulation is crucial, and in this study, a minimum regression coefficient ( $R^2$ ) of 0.992 is used in the development of correlations for the UDF from experimental data.

The higher the hysteresis of the PCM the more pronounced will be the advantages of the proposed methodology over the default enthalpy-porosity method employed by commercial software packages.

## **8.0 Acknowledgements**

This work was made possible through sponsorship from the Engineering and Physical Sciences Research Council (EPSRC) of the UK, Grant No: EP/H004181/1.

## 9.0 References

- [1] L. Shilei, F. Guohui, Z. Neng, D. Li, Experimental study and evaluation of latent heat storage in phase change materials wallboards, *Energy and Buildings* 39(2007): pp 1088 - 1091
- [2] F. Kuznik, J. Virgone, Jean Noel, Optimization of a phase change material wallboard for building use, *Applied Thermal Engineering* 29(2008): pp 1291-1298
- [3] F. Kuznik, J. Virgone, J.J Roux Energetic efficiency of a room wall containing PCM wallboard: A full scale experimental investigation, *Energy and Buildings*, 40(2008): pp 148-156
- [4] G. Susman, Z. Dehouche, T. Cheechern, S. Craig, Tests of prototype PCM 'sails' for office cooling, *Applied Thermal Engineering* 31(2010): pp 717-726
- [5] V.R Voller, L Shadabi, Enthalpy method for tracking a phase change boundary in two dimensions, *International Communications in Heat Mass Transfer* 11(1984): pp 239-249
- [6] ANSYS FLUENT Theory Guide (Release 13.0, November 2010), Solidification and melting, Ch 18: pp 569 -576
- [7] P.W Egolf, H Manz, Theory and modelling of phase change materials with and without mush regions, *International Journal of Heat and Mass Transfer* 37(1994): pp 2917 – 2624

- [8] S.C.K De Schepper, G.J Heynderickx, G.B Marin, Modeling the evaporation of a hydrocarbon feedstock in the convection section of a steam cracker, *Computers and Chemical Engineering* 33 (2009): pp 122–132
- [9] F. Kuznik, J. Virgone, Experimental investigation of wallboard containing phase change material: Data for validation of numerical modelling, *Energy and Buildings* 41 (2009): pp 561–570
- [10] D. Heim and J. Clarke, Numerical modelling and thermal simulation of phase change materials within ESP-r, Eighth International IBPSA Conference, Eindhoven, Netherlands, August 11-14, 2003
- [11] J. Bony, S Citherlet , Numerical model and experimental validation of heat storage with phase change materials, *Energy and Buildings* 39 (2007): pp 1065–1072
- [12] I. Ceróna, J. Neila, M. Khayet , Experimental tile with phase change materials (PCM) for building use, *Energy and Buildings* 43 (2011): pp 1869–1874
- [13] A. Lazaro, E. Gunther, H. Mehling, S. hiebler, JM. Marin, B. Zalba, Verification of a T-history installation to measure enthalpy versus temperature curves of phase change materials, *Measurement Science and Technology*, 17(2006): pp. 2168-2174
- [14] Chartered Institute of Building Services Engineers (CIBSE), Guide A (2006): pp. 3-48